Journal of Alloys and Compounds, 191 (1993) 71–78
JALCOM 452

The Au–Sn phase diagram

J. Ciulik* and M. R. Notis
Department of Materials Science and Engineering, Lehigh University, Bethlehem, PA 18015 (USA)

(Received January 29, 1992; in revised form July 30, 1992)

Abstract

The gold-rich side of the Au–Sn system has been examined using differential thermal analysis, differential scanning calorimetry and electron probe microanalysis. The presence of three intermetallic phases, β, ζ and ζ', between gold and AuSn has been verified, although the composition ranges reported here are significantly different from those of previous studies. The resulting proposed Au–Sn phase diagram contains six intermetallic compounds and seven invariant reactions.

Within the gold-rich region of the diagram there are four invariant reactions that occur: peritectics at 532 and 521 °C, a eutectic at 280 °C and a peritectoid at 190 °C, below which ζ' is stable. The solubility range of tin in the ζ phase at 280 °C is 9.5–17.6 at.% Sn and in the β phase is 8.25–9.11 at.% Sn at the same temperature.

1. Introduction

The determination of the Au–Sn phase diagram was undertaken as part of a study of phase equilibria and reaction kinetics within the Au–Sn–Cu–Pb system. Because many microelectronic packages are gold plated and are soldered using Pb–Sn solders, the growth of brittle intermetallic compounds that involve this phase system at soldered interfaces can lead to dramatically reduced joint strength and the premature failure of a microelectronic device may result. To understand the reaction kinetics and interfacial phase formation within this complicated quaternary system, it is necessary to understand the four ternary systems and six binary systems within the Au–Sn–Cu–Pb system. A review of the binary phase diagrams and the available literature revealed that a re-examination of the Au–Sn diagram was necessary, especially within the gold-rich region.

The Au–Sn binary system was evaluated by Okamoto and Massalski in 1984 [1]. However, subsequently published data [2, 3] cast doubt upon the phase boundaries and invariant reaction temperatures in the gold-rich region of the diagram. The most recent phase diagram for the Au–Sn system, again by Okamoto and Massalski [4], incorporates the results of Legendre *et al.* [2, 3] and shows the β and ζ phases to form by peritectic reactions at 532 and 519 °C respectively. However, the diagram by Okamoto and Massalski [4] still indicates the β phase to be unstable below about 220 °C, and the phase boundaries for the β and ζ phases are only approximated. Therefore clarification of this region of the diagram is needed.

To redetermine the gold-rich side of the equilibrium phase diagram, two-phase alloys and diffusion couples were analyzed by electron probe microanalysis (EPMA) and metallographic techniques. Single- and two-phase alloys were analyzed using differential thermal analysis (DTA) and differential scanning calorimetry (DSC).

2. Experimental details

2.1. Alloy preparation

Alloys were prepared from gold sponge (99.999%, Englehard Industries, Inc.) and tin shot (99.999%, Johnson Matthey, Inc). Initial alloy compositions of 7.5, 9.0, 14.0, 18.0 and 21.0 at.% Sn were prepared to lie within two-phase regions delineated by previously published phase diagrams. Standards of pure gold, tin and the compound AuSn were prepared for use as diffusion couple end members and EPMA standards.

Each component was weighed to the nearest 0.00001 g and placed in a high purity alumina crucible with the tin portion at the bottom of the crucible to reduce loss by vaporization. High frequency induction melting under a flowing argon atmosphere (approximately 300 $cm^3\ min^{-1}$) ensured homogenization. Each alloy (3–10 g per sample) was heated to approximately 1100 ± 25 °C as measured by an optical pyrometer and then cooled to room temperature.

*Present address: Radian Corporation, Mechanical and Materials Engineering Department, 8501 Mopac Boulevard, Austin, TX 78720, (USA)

0925-8388/93/$6.00

© 1993 – Elsevier Sequoia. All rights reserved

Each alloy with less than 18 at.% Sn was homogenized at 460 ± 0.8 °C for 200 h. Alloys of 18 and 21 at.% Sn were homogenized at 270 ± 0.8 °C for 100 h. The reported temperatures are accurate to ±2 °C because the thermocouple error contributed ±1.1 °C. The furnace temperature was monitored with a calibrated chromel–alumel thermocouple attached to each sample capsule. Individual samples were encapsulated in quartz tubing (for heat treatments at or above 400 °C) or glass tubing (for heat treatments below 400 °C) following repeated purging in argon and evacuation to approximately 50 mTorr.

After homogenization anneals the samples were quenched by crushing the capsules in cold water (about 10 °C). Sections approximately 2 mm thick were cut using a low speed diamond saw for further heat treatment, compositional evaluation, thermal analysis and microprobe analysis.

Heat treatment of the alloys was done at the temperatures listed in Table 1. Transfer time from the furnace to the quench bath was approximately 3 s, with less than 1 °C of cooling registering on the attached thermocouple before quenching occurred.

2.2. *Diffusion couples*

Fabrication of diffusion couples was attempted with the intention to cross the gold-rich end of the phase diagram from gold to AuSn (δ) and to duplicate the phase boundary data determined from two-phase alloys. Numerous attempts to bond couples between these end members were unsuccessful owing to the extreme brittleness of the compound AuSn. Because tightening of the diffusion couple clamp tended to shatter the AuSn, the end members were placed in intimate contact and only a small force was applied to the clamp to hold them together; not one of eight couples bonded. Diffusion couples between gold and tin bonded, but only AuSn (δ), $AuSn_2$ (ϵ) and $AuSn_4$ (η) compounds formed at the interface. Consequently, couples were made between gold and ζ, a less brittle phase than AuSn (δ) with considerable tin solubility (about 12–16 at.% Sn). Couples were successfully bonded at 400, 350, 300 and 210 °C for times corresponding to those used in the heat treatment of two-phase alloys (Table 1).

2.3. *Metallographic preparation*

Following heat treatment, each sample was mounted in epoxy cured at room temperature and ground through 600-grit SiC grinding paper using standard metallographic techniques. Grinding on 8, 3 and 1 μm SiC grinding paper followed, using a lubricant of paraffin in kerosene to reduce embedding of SiC particles in the gold-rich phases. Polishing with 1 μm diamond paste followed the grinding steps. Final polishing steps using 0.3 μm alumina followed by colloidal silica, both on Buehler automatic polishing equipment, yielded satisfactory specimens. An etchant of 40% HCl, 10% HNO_3 and 50% H_2O delineated the phases present in the alloys.

Accurate analysis by EPMA must be performed on a flat, polished but unetched specimen; consequently, the individual phases were marked with Vickers microhardness indentations (25 gf load) and the etched material was removed by polishing with 1 μm diamond paste. Final polishing using the automatic polisher left the samples with minimal surface relief and visible microhardness indentations. Microprobe traces between the indentations established tie-line concentrations if the alloy had reached equilibrium during the heat treatment. Samples that had not reached equilibrium were heat treated for longer times.

Diffusion couples were cut and ground to the approximate center of the couple and polished using the same procedure described above. Indentation marking

TABLE 1. Homogenization times and temperatures

Temperature (°C)	Time (h)					
	7.5 at.% Sn	9.0 at.% Sn	10.0 at.% Sn	14.0 at.% Sn	18.0 at.% Sn	21.0 at.% Sn
528.0 ± 0.8	75	75	75	75	–	–
520.0 ± 0.8	120	120	120	120	–	–
500.0 ± 0.8	120	120	120	120	–	–
460.0 ± 0.8	240	240	240	240	–	–
400.0 ± 1.5	360	360	360	360	–	–
350.0 ± 1.5	500	500	500	500	–	500
300.0 ± 0.8	800	800	800	800	–	–
270.0 ± 1.5	–	–	–	–	–	1000
250.0 ± 1.0	1000	1000	1000	1000	1000	1000
230.0 ± 0.8	–	–	–	–	–	1000
210.0 ± 1.2	1500	1500	1500	1500	1500	1500
190.0 ± 1.3	2000	2000	2000	2000	2000	2000
170.0 ± 1.5	2000	2000	2000	2000	2000	2000

was again necessary to delineate the diffusion interface region to be analyzed by EPMA.

2.4. Thermal analysis

Sections from each alloy, weighing between 10 and 50 mg, were cut for DSC samples. Samples of 80–200 mg were used for DTA. Each DSC sample was heated from the homogenization temperature (Table 1) to 550 °C at a rate of 0.5 °C min^{-1} in a calibrated Mettler TA3000 differential scanning calorimeter.

DTA studies were accomplished using a DuPont 9900 series differential thermal analyzer. Each sample was heated and cooled at 10 °C min^{-1} with nitrogen flowing through the sample chamber at 100 cm^3 min^{-1}. Reaction temperatures were reported as the onset of the reaction.

2.5. Electron probe microanalysis

EPMA was used to determine whether equilibrium had been established in the two-phase alloys and to measure the composition of each phase present in the alloys. An automated JEOL 733 microprobe equipped with a Tracor Northern 2000 computer system was used. A correction routine incorporated into the Sandia TASK8 operating program applied proper Z, A, F and $\Phi(\rho z)$ corrections to the X-ray intensity ratios using the formalism outlined in ref. 5.

The standards used to calibrate the microprobe were 99.999% Au and the compound AuSn (δ) that had been prepared from the same pure metals as the alloys. AuSn (δ) was used as a standard rather than tin because the alloys in this study were between gold and 21 at.% Sn and correction factors using AuSn (δ) as a tin standard were more reliable.

The composition of each phase present in an alloy was determined by point counting on the individual phase with a minimum of 50 determinations per phase. The operating conditions of the microprobe were as follows: 18 kV accelerating voltage, 150 nA beam current, 40° X-ray take-off angle and a 60 s counting time for both elements. The 18 kV accelerating voltage yields X-ray production depths of 1.0 μm for tin (L_α X-rays) and 0.4 μm for gold (M_α X-rays), according to the Anderson–Hasler equation [6]. A detailed description of the EPMA parameters and experimental procedure is contained in ref. 7.

In equilibrated two-phase alloys, where the composition was observed to be uniform across the phase, the average measured composition was calculated and the value was given as the equilibrium phase boundary. For diffusion couples, where a concentration gradient existed across each phase, the gradient curves were extrapolated to the visible interface and the interface values were taken as the equilibrium values [8].

Measurements made on high purity gold, tin and the compound AuSn (δ) were performed to determine the accuracy of the EPMA measurements. The analysis of 100 points on each sample yielded the following results: 100.05 ± 0.09 wt.% Au, 100.02 ± 0.06 wt.% Sn and 50.19 ± 0.22 at.% Sn in AuSn (δ).

3. Results and discussion

3.1. Microstructural features

Five types of two-phase microstructures were observed in this study: $\alpha+\beta$ (Fig. 1(a)), $\beta+\zeta$ (Fig. 2(a)), ζ+eutectic (Fig. (3a)), $\zeta+\delta$ (Fig. 4(a)) and $\zeta'+\delta$ (Fig. 5(a)). The α phase was easily recognizable as a heavily twinned phase in the $\alpha+\beta$ alloys. In the $\beta+\zeta$ alloys the ζ phase generally etched to a darker color while the β phase

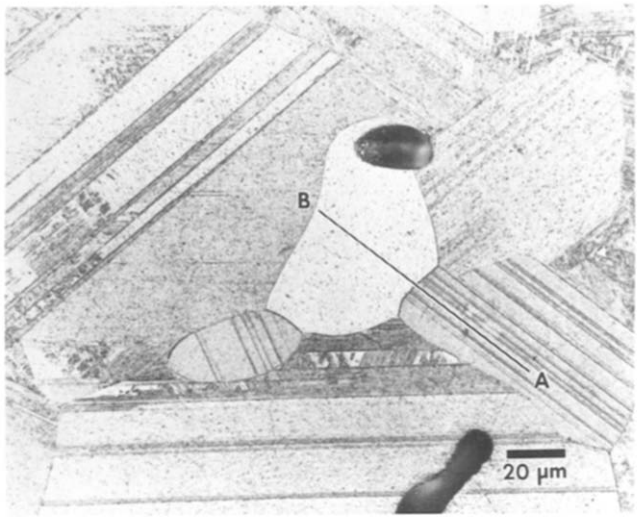

(a)

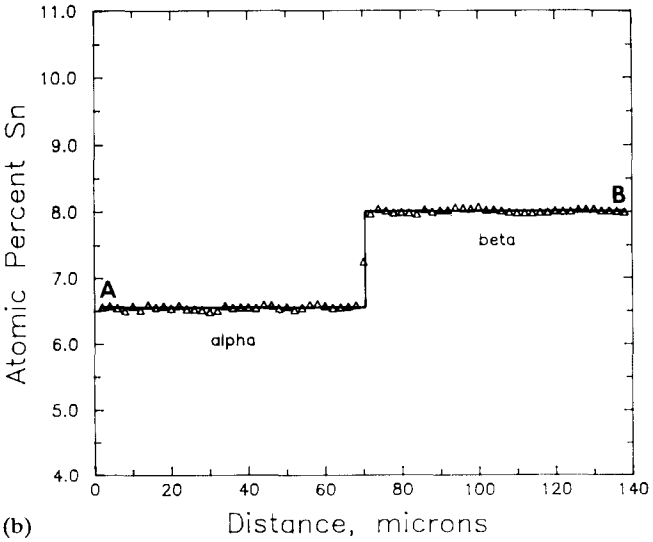

(b)

Fig. 1. Concentration profile across an α–β interface equilibrated at 528 °C.

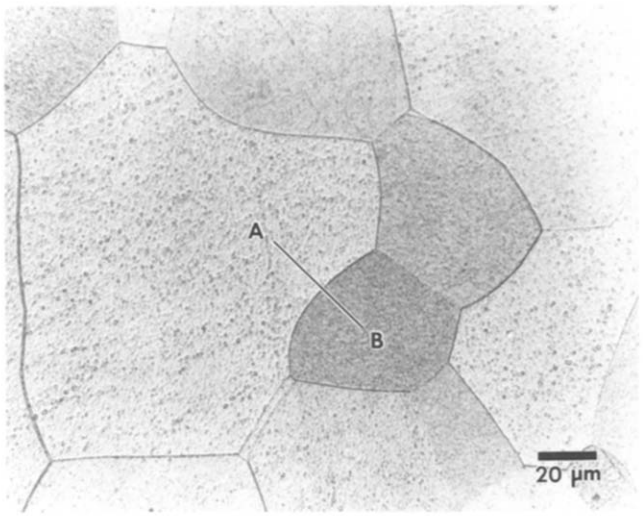

(a)

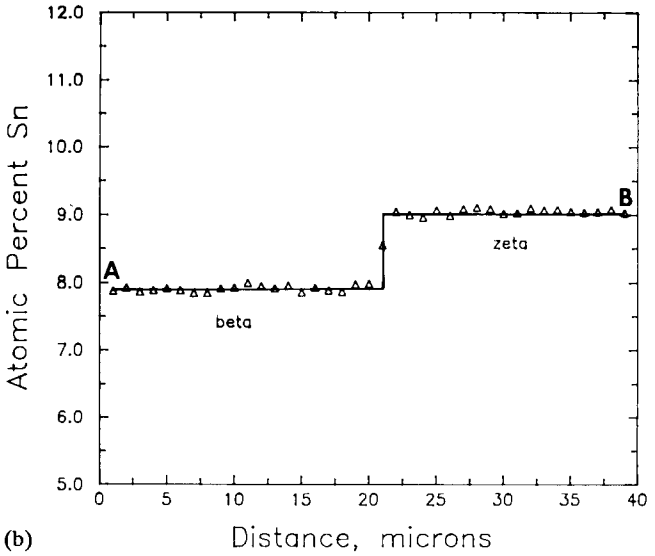

(b)

Fig. 2. Concentration profile across a β–ζ interface equilibrated at 460 °C.

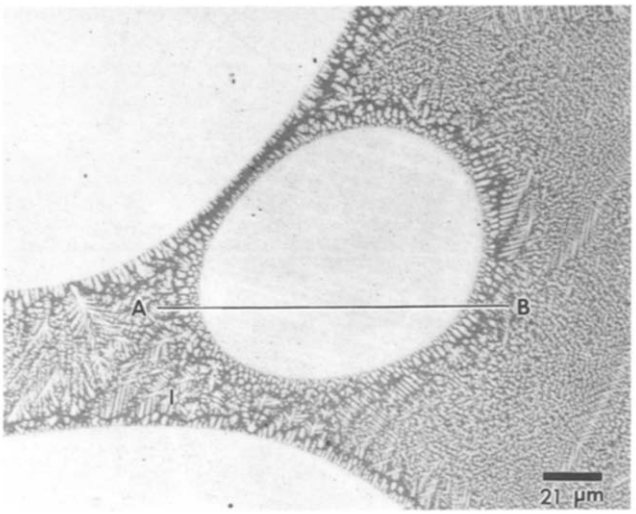

(a)

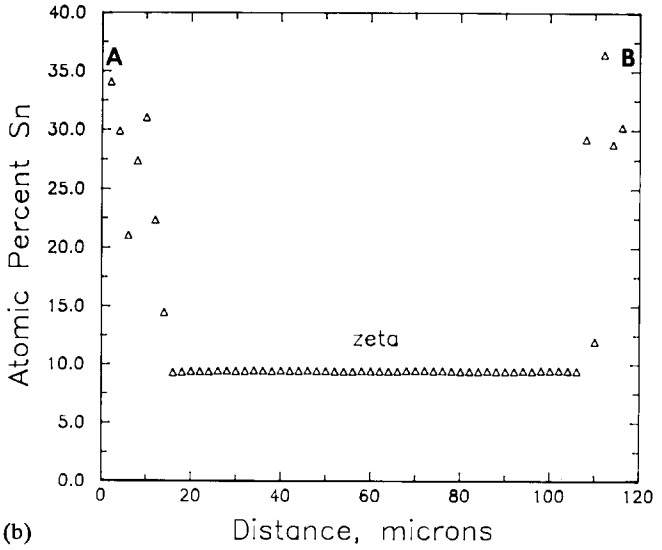

(b)

Fig. 3. Concentration profile across ζ–eutectic interfaces equilibrated at 520 °C.

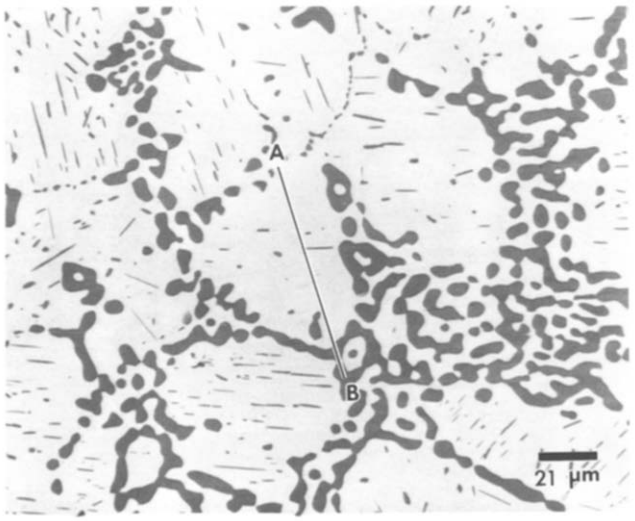

(a)

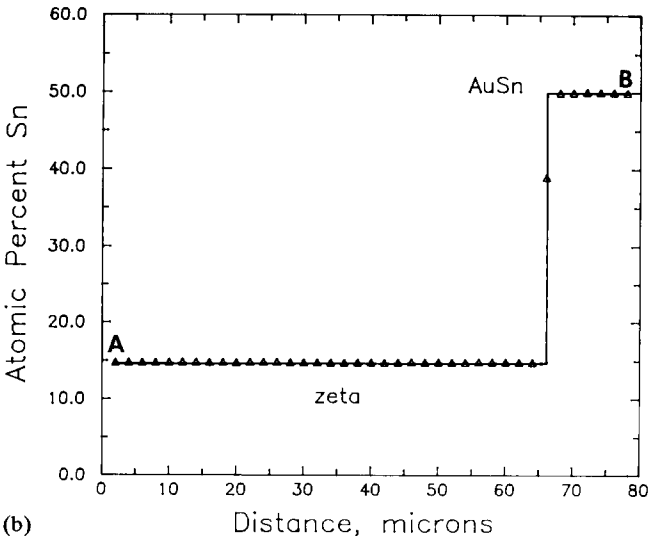

(b)

Fig. 4. Concentration profile across a ζ–δ interface equilibrated at 230 °C.

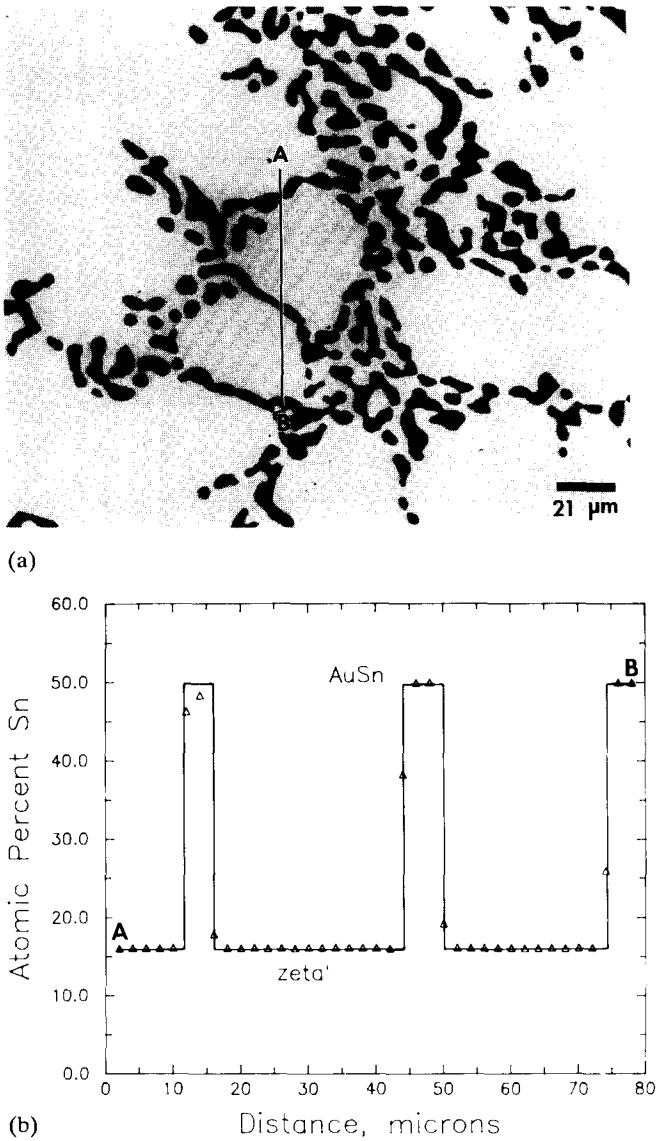

Fig. 5. Concentration profile across ζ–δ' interfaces equilibrated at 170 °C.

remained white. The ζ+eutectic alloys consisted of ζ phase particles in a matrix of the eutectic structure ($\zeta+\delta$). The eutectic alloys ($\zeta+\delta$) precipitated the δ phase within ζ phase grains as the eutectic alloys were heat treated at lower temperatures (Fig. 4(a)), indicating a decreasing solubility of tin and a corresponding increase in the volume fraction of δ phase present in the alloy. When the 190 °C reaction temperature was crossed, the δ phase was not visible as precipitates within ζ' phase grains (Fig. 5(a)), indicating that the ζ' phase was higher in tin content than the ζ phase.

3.2. Electron probe microanalysis

Concentration profiles across two-phase boundaries in equilibrated microstructures were used to determine phase boundary data. Typical profiles across two-phase boundaries within the microstructures listed above are contained in Figs. 1(b)–5(b). The step function profiles indicate properly equilibrated alloys and, therefore, accurate phase boundary data. Tabulated values of the phase boundary data are contained in Table 2.

TABLE 2. Errors associated with phase boundary points

Phase	Temperature (°C)	Composition (at.% Sn)	Standard deviation (at.% Sn)
α–β tie-lines			
α	528	6.57	0.07
β	528	8.02	0.05
α	520	6.45	0.18
β	520	7.99	0.10
α	500	6.39	0.14
β	500	7.91	0.11
α	460	5.95	0.09
β	460	7.74	0.14
α	400	5.58	0.22
β	400	7.65	0.08
α	350	5.44	0.14
β	350	7.58	0.12
α	300	5.39	0.10
β	300	7.57	0.06
β–ζ tie-lines			
β	520	7.99	0.06
ζ	520	9.04	0.08
β	500	8.02	0.09
ζ	500	9.10	0.15
β	460	8.06	0.12
ζ	460	9.16	0.11
β	400	8.14	0.14
ζ	400	9.26	0.17
β	350	8.17	0.19
ζ	350	9.31	0.13
β	300	8.32	0.06
ζ	300	9.34	0.13
β	250	8.40	0.11
ζ	250	9.58	0.23
β	210	8.53	0.13
ζ	210	9.56	0.13
β	190	8.15	0.07
ζ	190	9.62	0.05
ζ solidus points			
ζ	520	9.38	0.13
ζ	500	9.89	0.10
ζ	460	10.94	0.11
ζ	400	12.72	0.10
ζ	350	14.44	0.06
ζ solvus points			
ζ	270	16.46	0.08
ζ	250	16.06	0.08
ζ	230	14.77	0.11
ζ	210	14.20	0.10
ζ	190	14.11	0.07
ζ'	170	16.07	0.08

The error associated with each data point was taken as one standard deviation of the concentration obtained from the 50 analysis points (Table 2). Owing to the large number of X-ray counts obtained during each analysis, error values obtained through the use of X-ray counting statistics were too small to be considered appropriate (less than 0.03 at.%). The error bars associated with each data point based on the standard deviation of the concentrations measured are smaller than the symbols used in the figures.

Concentration profiles across four diffusion couple interfaces between gold and ζ phase resulted in phase boundary compositions very similar to those obtained from two-phase alloys. A typical profile is shown in Fig. 6. A tabulation of the phase boundary data obtained from the diffusion couples is presented in Table 3.

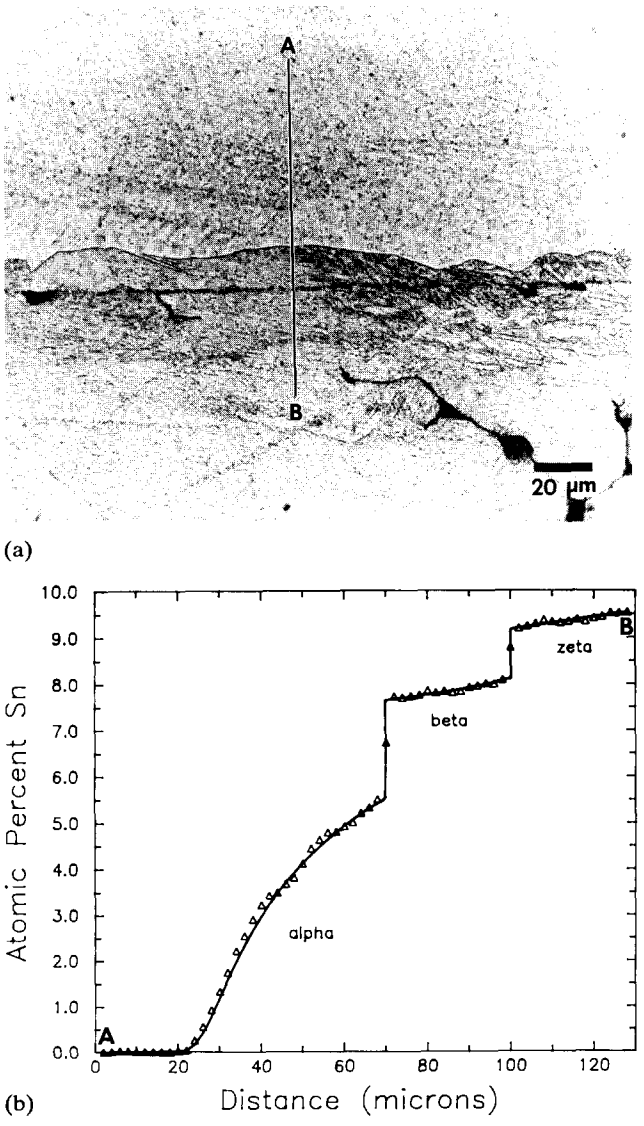

Fig. 6. Concentration profile across an Au–ζ diffusion couple equilibrated at 350 °C.

TABLE 3. Phase boundary data from diffusion couples

Temperature (°C)	Phase boundary	Composition (at.% Sn)
400	α–β	5.45–7.60
400	β–ζ	8.20–9.05
350	α–β	5.55–7.65
350	β–ζ	8.20–9.20
300	α–β	5.50–7.45
300	β–ζ	8.20–9.30
210	α–β	4.00–7.30
210	β–ζ	8.50–9.10

TABLE 4. Thermal analysis data

Composition (at.% Sn)	Temperature (°C)			
7.5 DSC data	529.3			
10.0	530.5,	521.0		
14.0	531.6,	521.6		
21.0	531.7,	–,	280.2	
7.5 DTA data (heating)	964.4,	531.6,	521.0	
9.0	921.1,	533.6,	518.8	
10.0	906.7,	534.7,	525.4	
14.0	–,	534.0,	528.7,	278.8
18.0	–,	533.4,	526.8	
21.0	–,	–,	–,	279.8
7.5 DTA data (cooling)	961.4,	520.5		
9.0	920.0,	519.8		
10.0	905.6			

3.3. Thermal analysis

The results from the DSC and DTA studies are summarized in Table 4. The DTA data contain liquidus points as well as invariant reaction points. The data indicate two peritectic reactions at 532 and 521 °C. These temperatures are in agreement with the temperatures published by Legendre *et al.* [2, 3]. The eutectic temperature of 280 °C is in agreement with all previously published values and the reaction at 190 °C may be identified with that reported by Osada *et al.* [9].

3.4. Revised Au–Sn phase diagram

From the collected experimental data a revised version of the Au–Sn phase diagram has been produced. The Au–AuSn section is shown in Fig. 7. The error bars associated with each data point are smaller than the symbols used. The complete diagram, based upon all previously published data to date and incorporating Fig. 7, is shown in Fig. 8. Phase boundaries are least-squares polynomial fit curves and lines through the data. The equations for the boundaries are listed in Table 5.

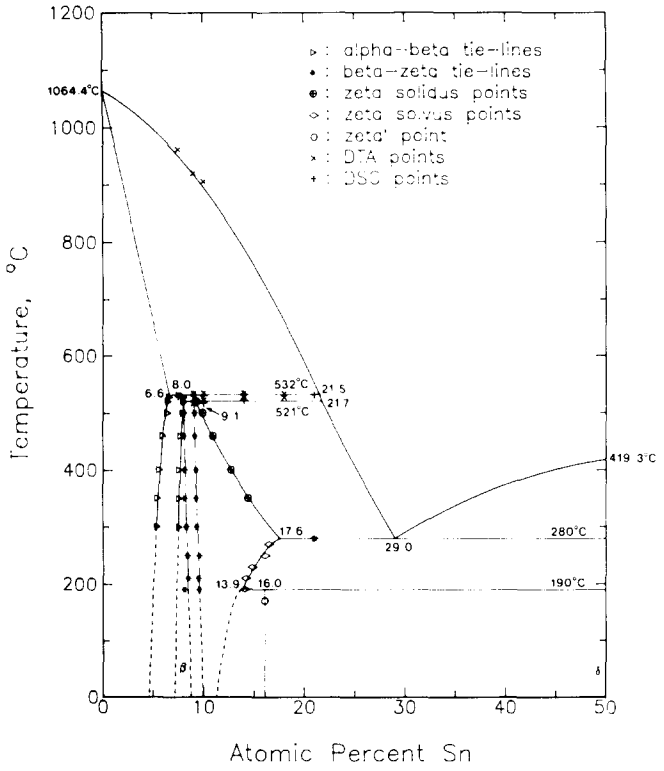

Fig. 7. The Au–AuSn phase diagram with data from this study.

TABLE 5. Fitting parameters for phase boundary curves $T=A+PX+CX^2$, where X is in at.% Sn

	A	B	C
Liquidus curve			
Au to 532 °C	1064.4000	−10.1021	−0.6820
532–521 °C	1714.4955	−54.9998	–
521–280 °C	1450.9108	−50.2161	0.3393
280–419.3 °C	−203.4365	22.4943	−0.2008
419.3–309 °C	21.8000	17.1250	−0.1835
309–252 °C	−319.0804	18.5784	−0.1370
252–217 °C	−9709.6613	225.2210	−1.2730
217 °C to Sn	−1257.6827	28.2566	−0.1336
Solidus curve			
α (Au)	1064.4300	−80.6712	–
ζ (521–280 °C)	951.6940	−56.5087	1.0391
δ (419.3–309 °C)	1.145E+4	−220.6	–
Solvus curve			
α (Au)	−4498.2603	1485.3679	−109.3764
β (Au rich)	-2.737×10^4	6747.4577	−407.5752
β (Sn rich)	5855.5099	−666.7187	–
ζ (521–0 °C)	5639.8302	−566.6127	–
ζ (280–190 °C)	−1247.3221	166.2232	−4.5126
ζ (190–0 °C)	−5023.5981	749.5158	−26.9375
δ (309–0 °C)	-3.090×10^4	618.0000	–

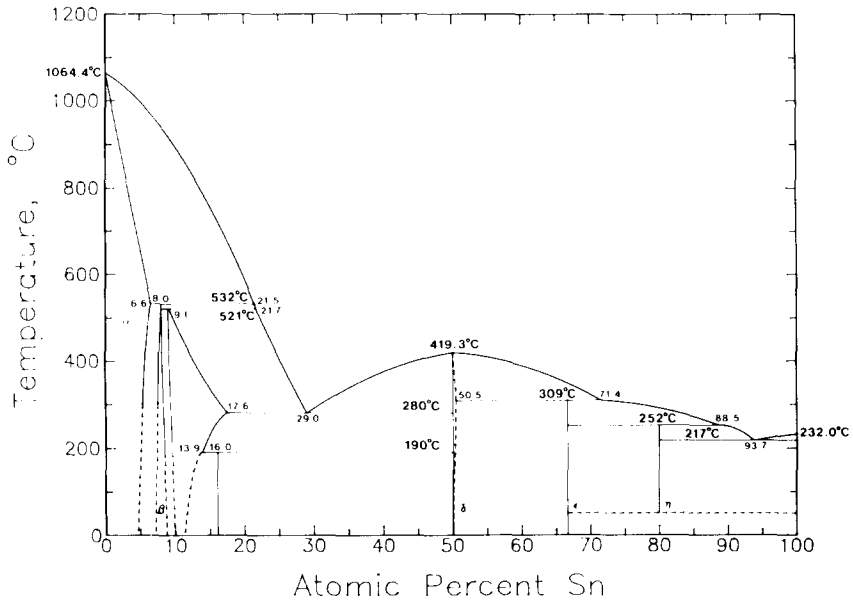

Fig. 8. The Au–Sn phase diagram.

The peritectic temperatures are in agreement with those of Legendre *et al.* [2, 3] and the composition of the ζ phase has hitherto been unpublished. One study [10] reported the β phase to be $Au_{10}Sn$ (9.09 at.% Sn), which differs significantly from the value obtained in this study (8.0 at.% Sn). A recent analysis by Butt and others [11] is in essential agreement with the results reported here, but their analysis did not report any solid solution range for the β phase, *i.e.* between 220 and 300 °C. They report it as a line compound at about 9 at.% Sn.

From the phase diagram (Fig. 8) it is evident that low temperature studies (below 190 °C) are necessary to determine whether the higher temperature phases extend to room temperature. Although both the β and ζ phases extend to at least 190 °C, the fact that room

temperature thin film studies [12–21] do not exhibit either phase does not necessarily indicate that they are not present in equilibrium microstructures. The kinetics of AuSn (δ) growth may suppress their formation.

4. Conclusions

(1) Two peritectic reactions occur at the gold-rich end of the Au–Sn phase diagram:

$\alpha + L \longrightarrow \beta$ (532 °C)

$\beta + L \longrightarrow \zeta$ (521 °C)

(2) Both the β and ζ phases are stable from their melting points to 190 °C and probably extend to room temperature.

(3) The ζ' phase has a composition of approximately 16.0 at.% Sn, with extended solubility, and forms from ζ through a peritectoid reaction at 190 °C.

Acknowledgments

The authors gratefully acknowledge the National Science Foundation for their support under NSF Grant DMR 8023955, Engelhard Industries for supplying the gold used in this study, Frank Prozonic of Air Products Corporation for the differential thermal analysis testing and Dr. W. F. Chambers of Sandia National Laboratories for customizing Sandia TASK8 for our microprobe.

References

1 H. Okamoto and T. B. Massalski, *Bull. Alloy Phase Diag., 5* (5) (1984) 492–503.
2 B. Legendre, C. Hancheng and A. Prince, *Bull. Soc. Chim. Fr., 1* (1985) I50–I57.
3 B. Legendre, C. Hancheng, F. Hayes, C. A. Maxwell, D. S. Evans and A. Prince, *Mater. Sci. Technol., 3* (1987) 875–876.
4 H. Okamoto and T. B. Massalski, *Binary Alloy Phase Diagrams,* ASM International, Metals Park, OH, 2nd edn., 1990, pp. 433–434.
5 W. F. Chambers, *Sandia Rep. SAN85-2037, Release UC-32,* 1985 (Sandia National Laboratories).
6 C. A. Anderson and M. F. Hasler, in R. Castaing, P. Deschamps and J. Philibert (eds.), *Optiques des Rayons X et Microanalyse,* Hermann, Paris, 1966.
7 J. Ciulik, *M.S. Thesis,* Lehigh University, Bethlehem, PA, 1988.
8 A. D. Romig Jr. and J. I. Goldstein, in G. C. Carter (ed.), *Applications of Phase Diagrams in Metallurgy and Ceramics, NBS Spec. Publ. 496,* 1978, p. 462.
9 K. Osada, S. Yamaguchi and H. Hirabayashi, *Trans. Jpn. Inst. Met., 15* (4) (1974) 256–260.
10 K. Schubert, H. Breimer and R. Gohle, *Z. Metallk., 50* (3) (1959) 146–153.
11 M. T. Butt, *Ph.D. Dissertation,* Brunel University, Uxbridge, 1991 (together with C. Bodsworth and A. Prince); M. T. Butt and A. Prince, personal communication, 1991.
12 K. Tu and R. Rosenberg, *Jpn. J. Appl. Phys., Suppl. 2,* Part 1 (1974) 633–636.
13 L. Buene, F. Finstad, K. Rimstad, O. Lonsjo and T. Olsen, *Thin Solid Films, 34* (1976) 149–152.
14 L. Buene, *Thin Solid Films, 43* (1977) 285–294.
15 L. Buene, *Thin Solid Films, 47* (1977) 159–166.
16 V. Simic and Z. Marinkovic, *J. Less-Common Met., 51* (1977) 177–179.
17 L. Buene and S.-T. Jacobsen, *Phys. Scr., 18* (1978) 397–399.
18 L. Buene, H. Falkenberg-Arell and J. Taftoe, *Thin Solid Films, 65* (1980) 247–257.
19 L. Buene, H. Falkenberg-Arell, J. Gjoennes and J. Taftoe, *Thin Solid Films, 67* (1980) 95–102.
20 S. Nakahara, R. J. McCoy, L. Buene and J. M. Vandenberg, *Thin Solid Films, 84* (1981) 185–186.
21 J. M. Vanderberg and R. A. Hamm, *Thin Film Interactions and Interfaces,* Electrochemical Society, Princeton, NJ, 1975, pp. 282–289.